Proxy reconstruction of ultraviolet-B irradiance at the Earth's surface, and its relationship with solar activity and ozone thickness

P. E. Jardine[1,2], W. T. Fraser[3,2], W. D. Gosling[4,2], C. N. Roberts[5], W. J. Eastwood[6] and B. H. Lomax[7]

[1]Institute of Geology and Palaeontology, University of Münster, 48149 Münster, Germany.

[2]School of Environment, Earth and Ecosystem Sciences, The Open University, Walton Hall, Milton Keynes, MK7 6AA, UK.

[3]Geography, Department of Social Sciences, Oxford Brookes University, Oxford OX3 0BP, UK.

[4]Department of Ecosystem and Landscape Dynamics, Institute of Biodiversity & Ecosystem Dynamics (IBED), University of Amsterdam, 1090 GE Amsterdam, The Netherlands.

[5]School of Geography, Earth and Environmental Sciences, University of Plymouth, PL4 8AA, UK.

[6]School of Geography, Earth and Environmental Sciences, University of Birmingham, B15 2TT, UK.

[7]Agriculture and Environmental Science, University of Nottingham, Sutton Bonington Campus, Leicestershire, LE12 5RD, UK.

Corresponding author:

Phillip Jardine, Institute of Geology and Palaeontology, University of Münster, 48149 Münster, Germany.

Email: Phillip Jardine (jardine@uni-muenster.de).

Abstract

26

27 Solar ultraviolet-B (UV-B) irradiance that reaches the Earth's surface acts as a biotic stressor

28 and has the potential to modify ecological and environmental functioning. The challenges of

29 reconstructing UV irradiance prior to the satellite era mean that there is uncertainty over long-

30 term surface UV-B patterns, especially in relation to variations in solar activity over

31 centennial and millennial timescales. Here, we reconstruct surface UV-B irradiance over the

32 last 650 years using a novel UV-B proxy based on the chemical signature of pollen grains.

33 We demonstrate a statistically significant positive relationship between the abundance of UV-

34 B absorbing compounds in *Pinus* pollen and modelled solar UV-B irradiance. These results

35 show that trends in surface UV-B follow the overall solar activity pattern over centennial

36 timescales, and that variations in solar output are the dominant control on surface level UV-B

37 flux, rather than solar modulated changes in ozone thickness. The *Pinus* biochemical response

38 demonstrated here confirms the potential for solar activity driven surface UV-B variations to

39 impact upon terrestrial biotas and environments over long timescales.

40

41 **Keywords**: Ultraviolet-B irradiance; pollen; vegetation; palaeoclimate; solar activity; ozone

42

Introduction

43

44 The role of solar activity in influencing the Earth system has received an increase in

45 attention over recent years (Ermolli et al., 2013; Gray et al., 2010; Solanki et al., 2013).

46 Predominantly, the focus has been on total solar irradiance (TSI, defined as the amount of

47 solar energy reaching the upper atmosphere) and its contributions to climatic changes versus

48 anthropogenic inputs (Solanki et al., 2013). In addition to TSI, which affects temperature and

49 atmospheric circulation patterns through 'bottom up' warming of the Earth's surface, there is

50 a growing awareness of the importance of ultraviolet (UV) irradiance as a climate forcing

51 mechanism (Gray et al., 2010; Ineson et al., 2015). UV irradiance stimulates production and

52 destruction of ozone via absorption driven processes (the Chapman cycle), resulting in a

53 warming of the stratosphere and exerting a 'top down' influence on regional climatic and

54 oceanic patterns through dynamical coupling with the underlying troposphere (Ermolli et al.,

55 2013; Gray et al., 2010; Ineson et al., 2015; Solanki et al., 2013).

56

57   Solar UV-B (280-315 nm) radiation that reaches the Earth's surface (referred to

58 hereafter as surface UV-B) is an important stressor on biotic systems, and has the potential to

59 drive larger-scale ecosystem-level processes (Rozema et al., 1997). As well as directly

60 damaging DNA, enhanced UV-B levels can lead to morphological and phenological changes

61 in plants and possibly alter competitive relationships among species (Caldwell et al., 1998;

62 Rozema et al., 1997). UV-B stimulates production of secondary metabolites that in part act as

63 UV protective compounds, which are both a metabolic cost to the plant and can influence

64 herbivory levels, plant decomposition and carbon cycling (Meijkamp et al., 1999; Rozema et

65 al., 1997). Increased surface UV-B can also directly enhance leaf litter decomposition through

66 photodegradation, and impact upon the activities of organisms such as animals, fungi and

67 bacteria that play a role in decomposition and nutrient cycling (Gehrke et al., 1995; Rozema

68 et al., 1997). While much attention has been focused on multidecadal increases in surface

69 UV-B flux due to anthropogenic reductions in ozone thickness (Caldwell et al., 1998; Lomax

70 et al., 2008), considerably less is known about the surface UV-B changes that result from long

71 term (centuries to millennia) variations in solar activity, and what impact these have on

72 ecological and environmental functioning.

73

74   Temporal changes in surface UV-B flux are a result of variations in solar UV

75 irradiance, ozone thickness, and their interaction. Variations in solar activity have been

76 characterized by satellite measurements since 1978 (all dates given in calendar years CE), and

77 historical proxies such as sunspot counts from 1610 and cosmogenic radionuclides (primarily

78 ^{10}Be and ^{14}C) through the Holocene (Solanki et al., 2013; Steinhilber et al., 2012; Svalgaard

79 and Schatten, 2016). These indicators reveal solar cycles ranging in length from ~27 days to

80 several millennia, as well as irregularly spaced, sustained 'Grand' minima and maxima of

81 solar activity (e.g. the Maunder Minimum, ~1645 to 1710) (Solanki et al., 2013; Usoskin,

82 2017). Temporal variations in solar UV irradiance are still poorly understood, partly because

83 of the discontinuous nature of spectral solar irradiance (SSI) satellite measurements

84 (Haberreiter et al., 2017), but mostly because of the challenges of reconstructing UV

85 irradiance beyond the satellite era. Nevertheless, SSI satellite measurements have revealed

86 UV cycles (in particular the 11-year solar cycle) in phase with those of TSI (Usoskin, 2017),

87 and the long term constancy of this relationship has been assumed in models of TSI and SSI

88 such as the semi-empirical SATIRE-T model (Spectral And Total Irradiance REconstructions

89 for the Telescope era), which has provided UV reconstructions back to the Maunder

90 Minimum (Krivova et al., 2010), and the empirical NRLSSI2 model (Naval Research

91 Laboratory Solar Spectral Irradiance), which has recently been extended back to 850 (Lean,

92 2018).

93

94   Increased UV-C (100-280 nm) flux during enhanced solar activity stimulates ozone

95 production, limiting the flow of UV-B to the Earth surface. It follows that while incoming

96 (top of atmosphere) UV-B and TSI may be correlated through time, surface level UV-B will

97 be anticorrelated with both (Rampelotto et al., 2009; Rozema et al., 2002), and this is

98 supported by ground based measurements of UV-B across the 11 year solar cycle

99 (Rampelotto et al., 2009). Rozema et al. (2002) hypothesized that this relationship will be

100 consistent across longer-term solar variations, with higher levels of surface UV-B flux during

101 solar activity lows such as the Maunder Minimum, even though overall UV and TSI are

102 reduced. Empirical evidence to test this hypothesis is currently lacking, however. Surface

103 UV-B proxy reconstructions based on the abundance of photoprotective pigments in fossil

104 cladocera (water flea) carapaces in arctic and subarctic lakes (Nevalainen et al., 2015, 2016,

105 2018) demonstrated a positive correlation between surface UV-B and solar activity over the

106 last millennium, which is the opposite pattern to that predicted by Rozema et al. (2002).

107 However, UV-B proxies based on aquatic organisms such as cladocerans are influenced by

108 water transparency as well as ambient UV-B, and so relate at least in part to local climatic and

109 vegetation conditions and anthropogenic land use changes (Nevalainen et al., 2015, 2018).

110 Although these impacts should have been limited in the arctic lake records used by

111 Nevalainen et al. (2016), where water and UV transparency are high, it is still not clear what

112 the long-term relationship between solar activity and surface UV-B is, and therefore what

113 biotic and environmental impacts can be expected from solar variability in the future.

114

115 　　　To address these uncertainties, we take advantage of a novel proxy for surface UV-B

116 irradiance based on the chemistry of pollen grains (Fraser et al., 2014; Rozema et al., 2001;

117 Seddon et al., 2019). Plants produce UV absorbing compounds (UACs) to protect their cells

118 from the harmful effects of UV-B, and up-regulate production in response to increased UV-B

119 doses (Fraser et al., 2014; Gao et al., 2004; Lomax et al., 2008; Rozema et al., 2001; Singh et

120 al., 2014). Pollen grains and spores preserve well in the fossil record because their outer wall,

121 or exine, is made of sporopollenin, a highly resistant biopolymer (Mackenzie et al., 2015).

122 Critically, the UAC signal within the exine is also preserved (Jardine et al., 2016), and

123 remains stable over geological time (Fraser et al., 2012). Therefore, by measuring the

124 concentration of UACs in fossil and sub-fossil pollen grains, UV-B flux in the past can be

125 reconstructed (Blokker et al., 2005, 2006; Fraser et al., 2014; Jardine et al., 2016; Lomax et

126 al., 2008; Rozema et al. 2001; Seddon et al., 2019; Willis et al., 2011).

127

128 　　　The UV-B response mechanism is thought to be an ancient evolutionary adaptation to

129 terrestrial environments and occurs across the land plant phylogeny (Christie et al., 2012;

Jardine et al., 2016; Rizzini et al., 2011; Rozema et al., 1997), which means that a wide array

of taxa are available for sampling from the pollen and spore record. To date, a positive

correlation between UV-B and sporopollenin UAC levels has been demonstrated for

Lycopodium (clubmoss) (Fraser et al., 2011; Jardine et al., 2016, 2017; Lomax et al., 2008,

2012; Watson et al., 2007), *Pinus* (pine) (Willis et al., 2011), *Cedrus atlantica* (Atlas cedar)

(Bell et al., 2018), *Vicia faba* (broad or fava bean) (Rozema et al., 2001), and Poaceae

(grasses) (Jardine et al., 2016), confirming the broad phylogenetic applicability of the UAC

proxy. Furthermore, because this proxy is based on terrestrial plants, it is less biased by

changes in the surrounding environment than those derived from aquatic organisms. UAC

concentrations in pollen and spores are determined by the UV dose experienced by the parent

plant, and are thought to represent the clear skies maximum UV level across the growing or

pollen/spore production period (i.e. a timescale of several weeks prior to pollen/spore release)

(Jardine et al., 2016; Lomax et al., 2012). The impact of short-term variations in cloudiness

on UAC levels should therefore be limited, and inter-annual comparisons of UV-B flux can

be achieved. Since the UAC proxy detects surface UV-B flux it is sensitive to changes in

ozone column thickness (Lomax et al., 2008), which means that variations in surface-level

UV-B caused by changes in ozone through time can be recovered.

Here, we use a maar lake sedimentary record from Nar Gölü in central Turkey, and

analyse UAC concentrations in *Pinus* pollen to reconstruct surface UV-B flux over the last

650 years. This record is then used to test for the correlation between surface UV-B and

modelled solar UV-B irradiance, following the assumption that TSI and solar UV-B

irradiance will vary in phase though time. A negative correlation would support the

hypothesis of Rozema et al. (2002), with solar activity highs leading to ozone production and

decreased UV-B flux to the surface. A positive correlation would support the cladoceran UV-

B reconstructions of Nevalainen et al., (2015, 2016, 2018), and would suggest that the

156 relationship between solar activity and ozone thickness observed on shorter timescales (e.g.

157 Rampelotto et al., 2009) cannot simply be scaled up across centuries and millennia.

158

159 **Materials and Methods**

160   Nar Gölü (38°20'24"N, 34°27'23"E; 1363 m a.s.l.) is a maar lake in central Turkey,

161 ~0.7 km^2 in area and ~26 m deep, with a sediment record extending through the Holocene and

162 into the last glacial (Dean et al., 2015). The upper 2500 years of the sedimentary sequence is

163 continuously annually laminated (varved), which has allowed for a precise chronology to be

164 developed (Dean et al., 2015; Jones et al., 2005). The Nar Gölü sediment record has been the

165 focus of previous sedimentological, mineralogical, palynological and geochemical research

166 (Dean et al., 2013, 2015; England et al., 2008; Jones et al., 2005, 2006).

167

168   The sediment core used in this study was collected in 2001, and the pollen samples

169 were initially documented in England et al. (2008). The age model for this core was based on

170 varve counting, which was carried out independently by two workers, who recounted until

171 agreement to within 3 laminae for each 6 cm section of core was reached (Jones et al., 2005).

172 Replication of varve counts from additional cores has provided a maximum age uncertainty of

173 2.5% of the given age (Jones et al., 2006). The pollen samples were collected at ~20 year

174 inter-sample resolution, with most samples representing 3 (sometimes 4 or 5) years of

175 sediment accumulation. The whole sequence covers 640 years and ~160 cm of sediment core.

176 The samples were processed according to standard palynological protocols, using 10% HCl,

177 10% NaOH, 60% HF, and acetolysis (England et al., 2008). We used the same pollen

178 preparations in this study to maintain stratigraphic consistency with the pollen count data, and

179 because standard processing protocols, including acetolysis (oxidation), do not impact upon

180 the recoverability of variations in UAC concentrations across samples (Jardine et al., 2015,

181   2016, 2017). Furthermore, Bell (2018) showed that UAC levels were similar in acetolysed

182   and untreated *Pinus* pollen.

183

184   We selected *Pinus* as the target taxon because it is abundant through most of the upper

185   part of the Nar Gölü record, with relative abundances of 13% to 45% of the pollen sum and

186   influx rates of 300 to 4400 cm^2/year (England et al., 2008). Furthermore, compared to lower

187   stature vegetation the impact of localized shading on UV reconstructions (Fraser et al., 2011;

188   Jardine et al., 2016) should be minimal. A positive association between UAC levels and UV-

189   B has also previously been demonstrated for *Pinus* pollen, across both a modern latitudinal

190   gradient and over the last 9.5 kyr (Willis et al., 2011), suggesting that a measurable signal is

191   recoverable from the Nar Gölü *Pinus* pollen record. *Pinus* pollen within the Nar Gölü

192   sediments represents mostly regional rather than local vegetation, and is mostly derived from

193   the Taurus Mountains >70 km south and southeast of Nar Gölü, although *Pinus* was also

194   planted near the lake in the 1980s (England et al., 2008). In the modern day, the three main

195   *Pinus* species in this region are *Pinus brutia*, *Pinus nigra* and *Pinus sylvestris* (Woldring and

196   Bottema, 2003), and these are anticipated to have been the major contributors to the Nar Gölü

197   *Pinus* pollen record during the study interval.

198

199   We used Fourier Transform Infrared (FTIR) microspectroscopy to generate the

200   chemical data, because previous analyses (Bell et al., 2018; Fraser et al., 2011; Jardine et al.,

201   2016, 2017; Lomax et al., 2008, 2012; Watson et al., 2007) have shown that this can

202   successfully capture variations in UAC abundances at small sample sizes. To prepare the

203   samples for FTIR analysis, individual *Pinus* pollen grains were picked out from the processed

204   sediment samples and mounted on ZnSe windows. To pick the pollen grains we used an

205   inverted microscope with a micromanipulator attachment, the full set-up comprising

206   Narishige MMN-1 and MMO-202ND course and fine control micromanipulators, an IM-11-2

207   pneumatic microinjector, with a Microtec IM-2 inverted microscope. The picked pollen grains

208   were arranged in groups of 4 to 5 grains on the ZnSe windows, with 5 replicate groups per

209   sample. This means that each FTIR spectrum represents 4 or 5 pollen grains, and each pollen

210   sample is represented by 5 replicate FTIR spectra. We generated the data using a Thermo

211   Scientific (Waltham, MA, USA) Nicolet Nexus FTIR bench unit connected to a Continuum

212   IR microscope fitted with an MCT-A liquid nitrogen-cooled detector and a Reflachromat 15x

213   objective lens. FTIR spectra were generated in transmission mode using a microscope

214   aperture of 100 x 100 μm recording the mean of 256 scans with a resolution of 1.928 cm^{-1}

215   wavenumbers. Five of the 33 samples in the study interval had insufficient *Pinus* pollen for

216   FTIR analysis, resulting in a dataset of 28 samples.

217

218   Peak height measurement and data analysis were carried out in R v3.4.0 (R Core

219   Team, 2017). The package 'baseline' v1.2-1 (Liland and Mevik, 2015) was used to baseline

220   correct the IR spectra, by subtracting a 2nd order polynomial baseline from each spectrum

221   (Figure 1). We quantified UAC concentrations by measuring the height of the 1510 cm^{-1}

222   aromatic (C=C) peak (Fig. 1), because this peak records changes in the abundance of the

223   phenolic compounds *para*-coumaric acid and ferulic acid that act as UACs in sporopollenin

224   (Fraser et al., 2014; Watson et al., 2007). Absorbance values in IR spectra relate to the

225   thickness of material being analysed, so following previous research (Fraser et al., 2011;

226   Jardine et al., 2015, 2016, 2017; Lomax et al., 2008, 2012) the 1510 cm^{-1} aromatic peak

227   height was normalized against the hydroxyl (OH) band centred on 3300 cm^{-1} (Figure 1).

228   Although the aromatic/OH ratio has not yet been calibrated to UAC concentrations or UV

229   levels, it does provide a successful proxy whereby higher aromatic/OH ratio values equate to

230   higher UV-B flux (Fraser et al., 2011; Jardine et al., 2016, 2017; Lomax et al., 2008, 2012).

231   Short-term variations in ambient UV-B flux experienced by the pollen-producing plants will

232   add noise to the UAC reconstruction; possible sources of additional variability are considered

233   in the Discussion. The raw data (sample ages and peak height measurements) are available for

234   download from figshare (Jardine et al., 2019). **[NB For review please used this private link**

235   **to access the data: https://figshare.com/s/45c1f29f1d76c1cbc01d].**

236

237   **[Insert Figure 1]**

238

239   We used the historical SSI reconstruction of Lean (2018) to obtain solar UV-B

240   irradiance estimates for the last 650 years. This SSI reconstruction covers the period 850 to

241   2016, and provides an annually resolved time series that incorporates information from space-

242   based irradiance observations, sunspots and cosmogenic radionuclides (full details in Lean

243   2018). Within the ultraviolet the SSI estimates are resolved to 1 nm wavebands. We therefore

244   integrated the irradiance values within the range 280 to 315 nm, to obtain an irradiance

245   reconstruction integrated across the UV-B part of the solar spectrum (shown in Figure 2b).

246

247   We used Spearman's rank order correlation to test the association between UACs and

248   solar UV-B. For the UACs we used the mean of the five replicates within each pollen sample,

249   and for solar UV-B we used the mean UV-B irradiance values within the calendar years

250   represented by each pollen sample. Spearman's rank order correlation is appropriate because

251   it is a non-parametric test that does not assume normality of distributions or a linear

252   relationship among variables. To examine the influence of shared long-term temporal trends

253   among the variables, we detrended the data by taking the residuals from linear regressions of

254   each variable against time. The residuals were then used as variables in the correlation test.

255

256   **Results**

257   The Nar Gölü *Pinus* UAC record (Figure 2a) shows that surface level UV-B irradiance

258   has varied over the last 650 years. Visual comparison with the solar UV-B reconstruction of

259   Lean (2018) (Figure 2b) reveals many of the same features, including an initial high value at

260   ~ 1350, minima at ~1460 to 1550 (the Spörer Minimum), 1645 to 1710 (the Maunder

261   Minimum), ~1790 to 1820 (the Dalton Minimum), and 1880 to 1920, and the rise from the

262   Maunder Minimum to the late 20th Century. The Spearman's rank order correlation between

263   the UAC data and solar UV-B reconstruction demonstrates statistically significant positive

264   relationships for both raw ($n = 28$, $r_s = 0.52$, $p = 0.005$) and detrended datasets ($n = 28$, $r_s =$

265   0.55, $p = 0.004$) (Figure 3). These correlations show that the visual similarities between the

266   surface and solar UV-B data are robust.

267

268   **[Insert Figure 2]**

269

270   **[Insert Figure 3]**

271

272   **Discussion**

273   Our results show a positive correlation between the *Pinus* UAC data and the solar UV-

274   B reconstruction of Lean (2018), demonstrating that solar activity and surface UV-B trends

275   have been concordant over the last 650 years. These results are in agreement with the

276   cladoceran-based surface UV-B reconstructions of Nevalainen et al. (2015, 2016, 2018), but

277   are not consistent with the hypothesis of Rozema et al. (2002) that surface level UV-B should

278   be anti-correlated with solar activity across grand solar minima and maxima. Our results

279   therefore suggest that any variations in the thickness of the ozone layer were not sufficient to

280   alter the incoming UV-B flux.

281

282   These results also demonstrate that the anti-correlation between solar activity and

283   ground-based measurements of UV across the 11 year solar cycle (Rampelotto et al., 2009)

284   cannot simply be scaled up to longer timescales (Rozema et al., 2002). Whether this implies a

285   different relationship between solar activity, UV and ozone thickness across the 11 year solar

286   cycle and longer-term cycles and trends is currently unclear. While solar UV irradiance at

287   wavelengths under 242 nm leads to ozone production, longer wavelength UV destroys it (Ball

288   et al., 2016), therefore given the right balance of change across the UV spectrum decreases in

289   ozone creation across solar minima could be cancelled out by decreases in ozone destruction

290   (and vice versa during solar maxima). Ozone concentrations are also modulated by hydrogen,

291   nitrogen, and chlorine catalytic cycles (Lary, 1997), and long-term variations in the

292   atmospheric concentrations of HOx, NOx and ClOx radicals may influence how ozone

293   thickness changes in response to solar UV. This question deserves further research, both with

294   more instrumental measurements of spectral UV irradiance and surface level UV-B, and

295   additional high-resolution UAC-based records over longer timescales.

296

297   While the relationships between our UAC data and solar UV-B are statistically

298   significant (Figure 3), the strength of the correlations are moderate ($r_s = 0.52$ for the raw data,

299   and $r_s = 0.55$ for the detrended data). In the Nar Gölü record we have identified three main

300   factors that, in addition to solar UV-B, may have been responsible for variation in the UAC

301   signal. First, the *Pinus* pollen does not represent local vegetation, but is thought to be largely

302   sourced from the Taurus Mountains (England et al., 2008). The pollen signal therefore likely

303   represents a mix of altitudes and incoming UV-B levels (Lomax et al., 2012), which will

304   contribute to within-sample variance (Seddon et al., 2019). To the extent that the UV-B

305   response differs among the *Pinus* species contributing pollen to the Nar Gölü record, any

306   variations in their relative abundances over time may have added further noise to the UAC

307   signal. The recently planted *Pinus* trees near Nar Gölü (England et al., 2008) may also have

308   impacted upon the UAC measurement from the most recent sample in the record, which

309   covers the years 1998 to 2001.

310

311   Second, variations in cloud cover modify surface UV irradiance levels (Calbó et al.,

312   2005; Fraser et al., 2011). Although the UAC proxy is unlikely to be affected by short-term

313   variations in cloudiness (Lomax et al., 2012), interannual variability in cloud cover may add

314   additional noise to UAC time series where each sample represents several years of pollen

315   release.

316

317   Third, any errors in the sediment core chronology will add noise to the correlations.

318   Although dating precision in the Nar Gölü record is thought to be better than the maximum

319   age uncertainty of 2.5% would suggest (Dean et al., 2013), small errors are likely to be

320   inevitable even in continuously varved sediments, and the magnitude of change in solar UV-B

321   irradiance across the 11 year solar cycle (Figure 2b; Lean, 2018) suggests that age model

322   deviations could add substantial noise to the UAC-UV relationship. While dating errors of a

323   few years could artificially impose a positive correlation between the solar UV-B

324   reconstruction and UAC data, the sustained, multi-decadal solar UV-B lows during both the

325   Spörer Minimum and Maunder Minimum (Figure 2b) coincide with intervals of low UAC

326   concentrations (Figure 2a). This suggests that the positive correlation demonstrated here is not

327   an artefact of minor errors in the varve chronology, but rather represents a genuine signal.

328

329   Despite these sources of variability, the UAC proxy has successfully recovered the

330   major solar UV-B signal, demonstrating that it has much to offer as a means of examining

331   solar inputs to the Earth system and their contributions to biotic and climatic change. As a

332   surface UV-B proxy UAC measurements allow us to test hypotheses relating to changes in

333   ozone thickness through time (Lomax et al., 2008), and can aid in deconvoluting the effects of

334   solar activity and ozone-related variations on UV-B at the Earth's surface. The pollen UAC

335   proxy could also be used in conjunction with UV proxies based on aquatic organisms

336   (Nevalainen et al., 2016) to separate out solar UV from water transparency effects

337 (Nevalainen et al., 2015, 2018), and therefore constrain key factors impacting on aquatic

338 ecosystems. More generally, the UAC proxy can be used to test for the impacts of surface

339 UV-B changes on biotic systems, in relation to solar UV irradiance variations, longer term

340 cycles in the Earth's orbit around the Sun (Jardine et al., 2016), and periods of ozone layer

341 disruption (Lomax et al., 2008; Visscher et al., 2004).

342

343   Our *Pinus* UAC data, taken together with the cladocera data of Nevalainen et al.

344 (2015, 2016, 2018), demonstrate that variations in solar UV irradiance are sufficient to drive

345 biochemical responses in disparate environments and groups of organisms. Future changes in

346 surface UV-B flux, whether driven by variations in solar activity or atmospheric composition,

347 will alter not just organismal stress but also the metabolic costs of producing UV protective

348 compounds, and may influence interspecific competitive relationships and ecosystem-level

349 processes such as decomposition and carbon cycling (Rozema et al., 1997). The relative

350 importance of these responses therefore needs to be assessed in future studies of ecological

351 change.

352

353 **Conclusions**

354   We have provided the first detailed proxy reconstruction of surface level UV-B flux

355 on centennial timescales. By linking this with a published solar UV-B reconstruction, we have

356 shown that solar UV-B flux at the surface follows a similar long-term trend to top of

357 atmosphere UV-B. On the timescales considered here, incoming solar UV flux will therefore

358 be the dominant control on surface-level UV, rather than UV modulated ozone thickness. In

359 addition to better understanding and modelling sources of variance in UAC reconstructions,

360 future research in this area needs to focus on calibrating the UAC UV-B proxy to a specific

361 dose-response relationship, to quantify the magnitude of change across different timescales

362 (Rozema et al., 2001, 2002, 2009; Seddon et al., 2019). Developing an action spectrum

363   (Herman, 2010; Rozema et al., 2001; Seddon et al., 2019) for UAC production will also be

364   important for quantifying how UAC concentrations vary with changes in ozone levels.

365   Together, these measures will help towards understanding how variations in solar UV

366   irradiance impact on Earth's climate and biota through time, both in the past and in the future.

367

377

378 **References**

379 Ball WT, Haigh JD, Rozanov EV, et al. (2016) High solar cycle spectral variations

380   inconsistent with stratospheric ozone observations. *Nature Geoscience* 9: 206-209.

381 Bell, BA. (2018) *Advancing the Application of Analytical Techniques in the Biological*

382   *Chemistry of Sporopollenin: Towards Novel Plant Physiological Tracers in*

383   *Quaternary Palynology*. PhD Thesis, University of Manchester, UK.

384 Bell BA, Fletcher WJ, Ryan P, et al. (2018) UV-B-absorbing compounds in modern *Cedrus*

385   *atlantica* pollen: The potential for a summer UV-B proxy for Northwest Africa. *The*

386   *Holocene* 28: 1382-1394.

387 Blokker, P, Boelen, P, Broekman, R and Rozema, J. (2006) The occurrence of *p*-coumaric

388   acid and ferulic acid in fossil plant materials and their use as UV-proxy. *Plant Ecology*

389   182: 197-207.

390 Blokker, P, Yeloff, D, Boelen, P, Broekman, R and Rozema, J. (2005). Development of a

391   proxy for past surface UV-B irradiation: A thermally assisted hydrolysis and

392   methylation py-GC/MS method for the analysis of pollen and spores. *Analytical*

393   *Chemistry* 77: 6026-6031.

394 Calbó J, Pagès D and González J-A. (2005) Empirical studies of cloud effects on UV

395   radiation: A review. *Reviews of Geophysics* 43.

396 Caldwell MM, Björn LO, Bornman JF, et al. (1998) Effects of increased solar ultraviolet

397   radiation on terrestrial ecosystems. *Journal of Photochemistry and Photobiology B:*

398   *Biology* 46: 40-52.

399 Christie JM, Arvai AS, Baxter KJ, et al. (2012) Plant UVR8 photoreceptor senses UV-B by

400   tryptophan-mediated disruption of cross-dimer salt bridges. *Science* 335: 1492-1496.

401 Dean JR, Jones MD, Leng MJ, et al. (2015) Eastern Mediterranean hydroclimate over the late

402   glacial and Holocene, reconstructed from the sediments of Nar lake, central Turkey,

403   using stable isotopes and carbonate mineralogy. *Quaternary Science Reviews* 124:

404   162-174.

405 Dean JR, Jones MD, Leng MJ, et al. (2013) Palaeo-seasonality of the last two millennia

406   reconstructed from the oxygen isotope composition of carbonates and diatom silica

407   from Nar Gölü, central Turkey. *Quaternary Science Reviews* 66: 35-44.

408 England A, Eastwood WJ, Roberts CN, et al. (2008) Historical landscape change in

409   Cappadocia (central Turkey): a palaeoecological investigation of annually laminated

410   sediments from Nar lake. *The Holocene* 18: 1229-1245.

Ermolli I, Matthes K, Dudok de Wit T, et al. (2013) Recent variability of the solar spectral irradiance and its impact on climate modelling. *Atmospheric Chemistry and Physics* 13: 3945-3977.

Fraser WT, Lomax BH, Jardine PE, et al. (2014) Pollen and spores as a passive monitor of ultraviolet radiation. *Frontiers in Ecology and Evolution* 2.

Fraser WT, Scott AC, Forbes AES, et al. (2012) Evolutionary stasis of sporopollenin biochemistry revealed by unaltered Pennsylvanian spores. *New Phytologist* 196: 397-401.

Fraser WT, Sephton MA, Watson JS, et al. (2011) UV-B absorbing pigments in spores: biochemical responses to shade in a high-latitude birch forest and implications for sporopollenin-based proxies of past environmental change. *Polar Research* 30: 8312.

Gao W, Zheng Y, Slusser JR, et al. (2004) Effects of Supplementary Ultraviolet-B lrradiance on Maize Yield and Qualities: A Field Experiment. *Photochemistry and Photobiology* 80: 127-131.

Gehrke C, Johanson U, Callaghan TV, et al. (1995) The impact of enhanced ultraviolet-B radiation on litter quality and decomposition processes in *Vaccinium* leaves from the Subarctic. *Oikos* 72: 213-222.

Gray LJ, Beer J, Geller M, et al. (2010) Solar Influences on Climate. *Reviews of Geophysics* 48.

Haberreiter M, Schöll M, Dudok de Wit T, et al. (2017) A new observational solar irradiance composite. *Journal of Geophysical Research: Space Physics* 122: 5910-5930.

Herman JR. (2010) Use of an improved radiation amplification factor to estimate the effect of total ozone changes on action spectrum weighted irradiances and an instrument response function. *Journal of Geophysical Research* 115.

Ineson S, Maycock AC, Gray LJ, et al. (2015) Regional climate impacts of a possible future grand solar minimum. *Nature Communications* 6: 7535.

437   Jardine PE, Abernethy FAJ, Lomax BH, et al. (2017) Shedding light on sporopollenin

438   chemistry, with reference to UV reconstructions. *Review of Palaeobotany and*

439   *Palynology* 238: 1-6.

440   Jardine PE, Fraser, WT, Gosling, WD, et al. (2019) Data from "Reconstruction of ultraviolet-

441   B irradiance at the Earth's surface, and its relationship with solar activity and ozone

442   thickness". figshare, https://dx.doi.org/10.6084/m9.figshare.8075519.

443   Jardine PE, Fraser WT, Lomax BH, et al. (2015) The impact of oxidation on spore and pollen

444   chemistry. *Journal of Micropalaeontology* 34: 139-149.

445   Jardine PE, Fraser WT, Lomax BH, et al. (2016) Pollen and spores as biological recorders of

446   past ultraviolet irradiance. *Scientific Reports* 6: 1-8.

447   Jones MD, Leng MJ, Roberts CN, et al. (2005) A Coupled Calibration and Modelling

448   Approach to the Understanding of Dry-Land Lake Oxygen Isotope Records. *Journal*

449   *of Paleolimnology* 34: 391-411.

450   Jones MD, Roberts CN, Leng MJ, et al. (2006) A high-resolution late Holocene lake isotope

451   record from Turkey and links to North Atlantic and monsoon climate. *Geology* 34:

452   361.

453   Krivova NA, Vieira LEA and Solanki SK. (2010) Reconstruction of solar spectral irradiance

454   since the Maunder minimum. *Journal of Geophysical Research* 115.

455   Lary DJ. (1997) Catalytic destruction of stratospheric ozone. *Journal of Geophysical*

456   *Research: Atmospheres* 102: 21515-21526.

457   Lean JL. (2018) Estimating Solar Irradiance Since 850 CE. *Earth and Space Science* 5: 133-

458   149.

459   Liland KH and Mevik B-H. (2015) baseline: Baseline Correction of Spectra. 1.2-1 ed.

460   Lomax BH, Fraser WT, Harrington G, et al. (2012) A novel palaeoaltimetry proxy based on

461   spore and pollen wall chemistry. *Earth and Planetary Science Letters* 353-354: 22-28.

462   Lomax BH, Fraser WT, Sephton MA, et al. (2008) Plant spore walls as a record of long-term

463   changes in ultraviolet-B radiation. *Nature Geoscience* 1: 592-596.

464   Mackenzie G, Boa AN, Diego-Taboada A, et al. (2015) Sporopollenin, The Least Known Yet

465   Toughest Natural Biopolymer. *Frontiers in Materials* 2: 1-5.

466   Meijkamp B, Aerts R, van de Staaij J, et al. (1999) Effects of UV-B on secondary metabolites

467   in plants. In: Rozema J (ed) *Stratospheric ozone depletion: The effects of enhanced*

468   *UV-B on terrestrial ecosystems.* Leiden: Backhuys, 71-99.

469   Nevalainen L, Luoto TP, Rantala MV, et al. (2015) Role of terrestrial carbon in aquatic UV

470   exposure and photoprotective pigmentation of meiofauna in subarctic lakes.

471   *Freshwater Biology* 60: 2435-2444.

472   Nevalainen L, Rantala MV, Luoto TP, et al. (2016) Long-term changes in pigmentation of

473   arctic Daphnia provide potential for reconstructing aquatic UV exposure. *Quaternary*

474   *Science Reviews* 144: 44-50.

475   Nevalainen L, Rantala MV, Rautio M, et al. (2018) Spatio-temporal cladoceran

476   (Branchiopoda) responses to climate change and solar radiation in subarctic ecotonal

477   lakes. *Journal of Biogeography* 45: 1954-1965.

478   Rampelotto PH, da Rosa MB and Schuch NJ. (2009) Solar cycle and UV‐B comparison for

479   South America−South of Brazil (29° S, 53° W). In: Nakajima T and Yamasoe MA

480   (eds) *AIP Conference Proceedings.* AIP, 490-493.

481   R Core Team (2017) R: A language and environment for statistical computing. 3.4.2 ed.

482   Vienna, Austria: R Foundation for Statistical Computing.

483   Rizzini L, Favory JJ, Cloix C, et al. (2011) Perception of UV-B by the *Arabidopsis* UVR8

484   Protein. *Science* 332: 103-106.

485   Rozema J, Blokker P, Mayoral Fuertes MA, et al. (2009) UV-B absorbing compounds in

486   present-day and fossil pollen, spores, cuticles, seed coats and wood: evaluation of a

487   proxy for solar UV radiation. *Photochemical and Photobiological Sciences* 8: 1233-

488   1243.

489   Rozema J, Broekman RA, Blokker P, et al. (2001) UV-B absorbance and UV-B absorbing

490   compounds (*para*-coumaric acid) in pollen and sporopollenin: the perspective to track

491   historic UV-B levels. *Journal of Photochemistry and Photobiology B: Biology* 62:

492   108-117.

493   Rozema J, van de Staij J, Björn L-O, et al. (1997) UV-B as an environmental factor in plant

494   life: stress and regulation. *Trends in Ecology and Evolution* 12: 22-28.

495   Rozema J, van Geel B, Björn L-O, et al. (2002) Toward Solving the UV Puzzle. *Science* 296:

496   1621-1622.

497   Seddon AWR, Festi D, Robson TM, et al. (2019) Fossil pollen and spores as a tool for

498   reconstructing ancient solar-ultraviolet irradiance received by plants: an assessment of

499   prospects and challenges using proxy-system modelling. *Photochemical and*

500   *Photobiological Sciences* 18: 275-294.

501   Singh SK, Reddy KR, Reddy VR, et al. (2014) Maize growth and developmental responses to

502   temperature and ultraviolet-B radiation interaction. *Photosynthetica* 52: 262-271.

503   Solanki SK, Krivova NA and Haigh JD. (2013) Solar Irradiance Variability and Climate.

504   *Annual Review of Astronomy and Astrophysics* 51: 311-351.

505   Steinhilber F, Abreu JA, Beer J, et al. (2012) 9,400 years of cosmic radiation and solar

506   activity from ice cores and tree rings. *Proceedings of the National Academy of*

507   *Sciences* 109: 5967-5971.

508   Svalgaard L and Schatten KH. (2016) Reconstruction of the Sunspot Group Number: The

509   Backbone Method. *Solar Physics* 291: 2653-2684.

510   Usoskin IG. (2017) A history of solar activity over millennia. *Living Reviews in Solar Physics*

511   14.

512 Visscher H, Looy CV, Collinson ME, et al. (2004) Environmental mutagenesis during the

513   end-Permian ecological crisis. *Proceedings of the National Academy of Sciences of the*

514   *United States of America* 101: 12952-12956.

515 Watson JS, Septhon MA, Sephton SV, et al. (2007) Rapid determination of spore chemistry

516   using thermochemolysis gas chromatography-mass spectrometry and micro-Fourier

517   transform infrared spectroscopy. *Photochemical and Photobiological Sciences* 6: 689-

518   694.

519 Willis KJ, Feurdean A, Birks HJB, et al. (2011) Quantification of UV-B flux through time

520   using UV-B-absorbing compounds contained in fossil Pinus sporopollenin. *New*

521   *Phytologist* 192: 553-560.

522 Woldring, H and Bottema, S. (2003) The vegetation history of east-central Anatolia in

523   relation to Archaeology: the Eski Acégöl pollen evidence compared with the Near

524   Eastern environment. *Palaeohistoria* 43/44: 1-31.

525
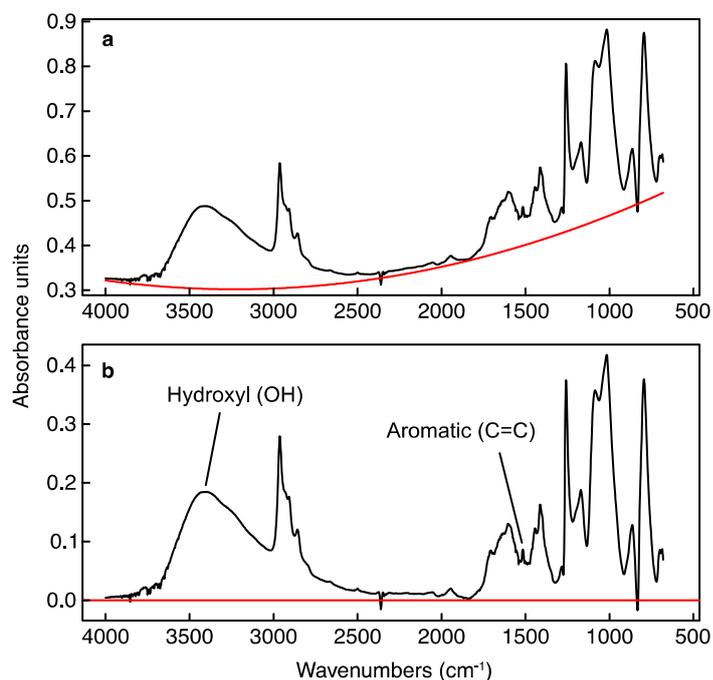
Figures

Figure 1. Representative chemical spectra of Nar Gölü *Pinus* pollen, from a sample dating

from 1741 CE. (a) uncorrected spectrum showing fitted 2nd order polynomial baseline. (b)

baseline corrected spectrum. The 1510 cm^{-1} aromatic peak represents UV-B absorbing

compounds (UACs) within pollen grains, and the 3300 cm^{-1} hydroxyl band is used to

normalize the peak height measurement.

534
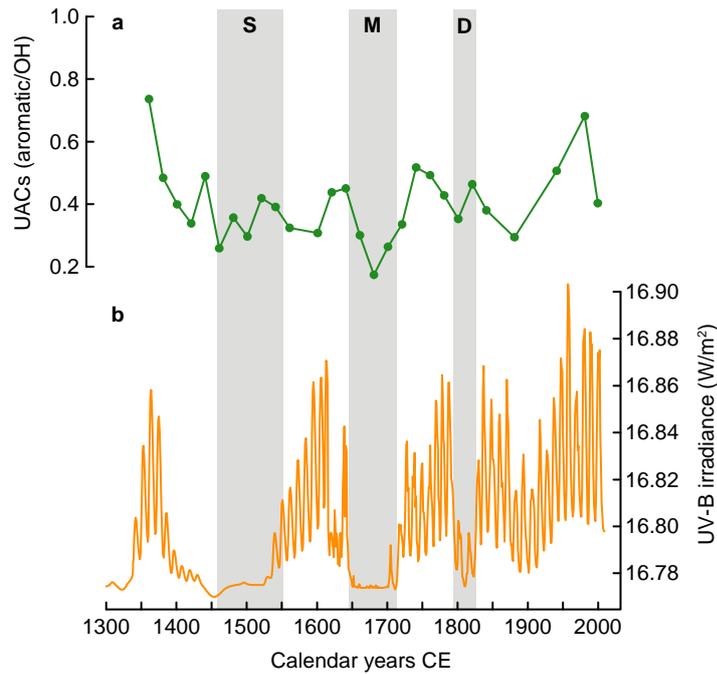
Figure 2. Surface and solar UV-B records. (a) Pinus UAC data from Nar Gölü, shown as the

mean of five replicates (solid green line with points showing samples) ±1 standard deviation

(shaded area). (b) Modeled solar UV-B irradiance, from Lean (2018). Grey shaded regions

show solar minima, D = Dalton Minimum, M = Maunder Minimum, S = Spörer Minimum.

539
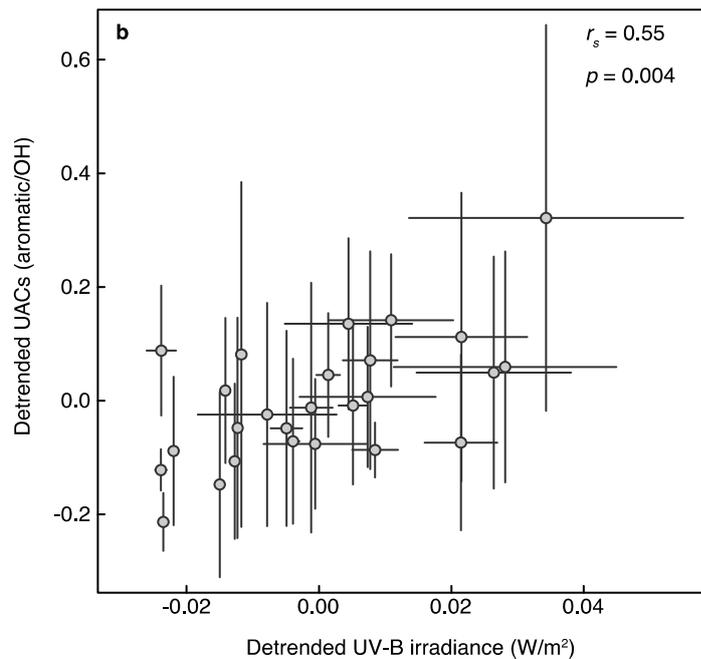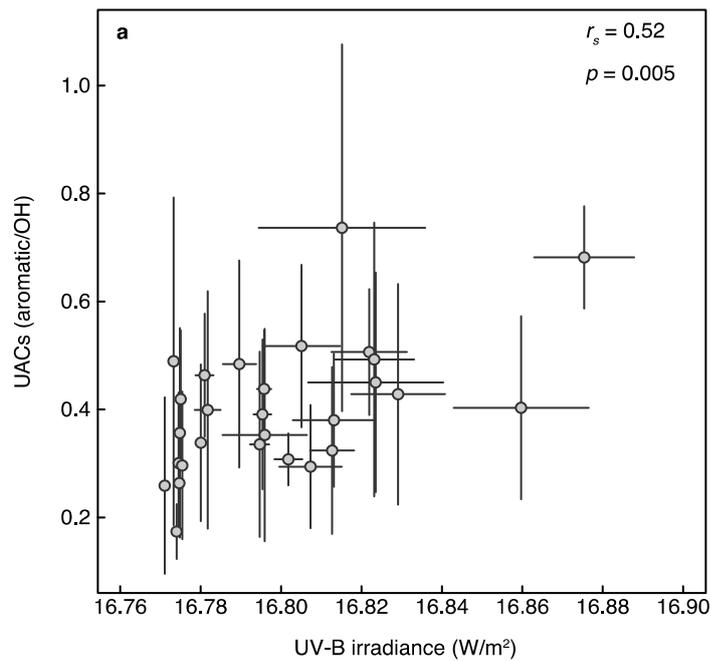
Figure 3. *Pinus* UAC data plotted against modeled solar UV-B irradiance (Lean 2018), for

both raw (a) and detrended (b) data. For the UAC data, the points show the mean of five

replicates, and the error bars are 1 standard deviation. For the UV-B irradiance reconstruction,

the points are the mean values within the calendar years represented by each pollen sample,

and the error bars are 1 standard deviation. r_s = Spearman's rank order correlation coefficient,

p = p value of correlation.